Asociación Argentina
de Mecánica Computacional

Mecánica Computacional Vol XXXI, págs. 899-923 (artículo completo)
Alberto Cardona, Paul H. Kohan, Ricardo D. Quinteros, Mario A. Storti (Eds.)
Salta, Argentina, 13-16 Noviembre 2012

A PARAMETRIC STUDY ON NONLINEAR ELASTODYNAMICS USING ISOGEOMETRIC ANALYSIS AND A DISSIPATIVE ENERGY-MOMENTUM CONSERVING ALGORITHM

Luis Felipe R. Espath[a], Alexandre L. Braun[b], Armando M. Awruch[c]

[a]*Graduate student, Graduate Program in Civil Engineering (PPGEC), Federal University of Rio Grande do Sul (UFRGS), Av. Osvaldo Aranha 99, 90035-190, Porto Alegre-RS, Brasil, espath@gmail.com, http://www.ufrgs.br/engcivil/ppgec/*

[b]*Professor, Graduate Program in Civil Engineering (PPGEC), Federal University of Rio Grande do Sul (UFRGS), Av. Osvaldo Aranha 99, 90035-190, Porto Alegre-RS, Brasil, allbraun@ig.com.br, http://www.ufrgs.br/engcivil/ppgec/*

[c]*Professor, Graduate Program in Civil Engineering (PPGEC), Federal University of Rio Grande do Sul (UFRGS), Av. Osvaldo Aranha 99, 90035-190, Porto Alegre-RS, Brasil, amawruch@ufrgs.br, http://www.ufrgs.br/engcivil/ppgec/*

Keywords: Isogeometric Analysis, Non-Uniform Rational B-Splines (NURBS), Nonlinear Elastodynamics.

Abstract. A parametric study is performed in this work in order to investigate the computational performance of a numerical model based on isogeometric analysis for applications in nonlinear elastodynamics. It is well known that finite element models cannot represent accurately the higher vibration modes of a dynamic response due to deficiencies associated with the spatial discretization procedure. In addition, time integration algorithms with unconditional stability in the linear range are frequently subject to numerical instability when they are applied to nonlinear problems. In this sense, it is expected that a formulation utilizing isogeometric analysis and a dissipative energy-momentum conserving scheme for time discretization can significantly improve numerical stability. In the present paper, a numerical model for dynamic analysis is presented considering the isogeometric formulation based on NURBS (non-uniform rational B-splines). The kinematical description is performed using the corotational approach formulated in the context of isogeometric analysis and the constitutive equation is written in terms of corotational variables according to the hypoelastic theory, where the small strain hypothesis is adopted. Large displacements and large rotations may be also considered in the present scheme. A dissipative energy-momentum conserving algorithm is adopted to solve the equation of motion by using the generalized-α method and algorithmic conservation of energy as well as linear and angular momentum. Numerical examples are analyzed with the numerical formulation proposed in this work and results are compared with predictions obtained from a finite element model in order to quantify computational aspects such as efficiency and accuracy.

1 INTRODUCTION

Isogeometric analysis can be interpreted as a numerical procedure to unify numerical techniques associated with geometrical design and analysis by employing a single parameterization framework, where the same basis functions are utilized throughout the numerical modeling. Geometrical design and analysis have been performed independently with pre-processing programs based on computer aided design (CAD) technologies and numerical solvers based on the finite element method (FEM). However, it is frequently observed that the finite element model obtained after mesh generation cannot match the geometric shape of complex models reproduced with CAD tools, since insufficient approximations may be utilized depending on the basis functions adopted in the finite element formulation and the number of elements used in the spatial discretization. Extending this remark to the field of dynamic analysis, one can also observe that the higher vibration modes of a dynamic response cannot be accurately represented due to modeling errors introduced when the spatial discretization procedure is applied to infinite-dimensional continuum systems, which may give rise to numerical instabilities if numerical dissipation is not adequately employed. In order to circumvent this drawback, isogeometric analysis may be utilized, where B-splines and NURBS are adopted to build the geometric models and to approximate the solution field.

Numerical models with controllable dissipation were firstly developed to stabilize time discretization procedures referring to dynamic systems, especially for linear applications. The Newmark's method, for instance, presented no numerical dissipation in its standard form, but a formulation with controllable numerical damping was also proposed in Newmark (1959). By studying the Newmark's method and other early algorithms with numerical dissipation, such as the Wilson's method and the Houbolt's method, Goudreau and Taylor (1973) concluded that some amount of damping must be introduced in the numerical schemes to reduce the spurious action of higher vibration modes. However, it is well known that second-order accuracy is lost when numerical dissipation is considered. In this sense, Hilber et al. (1977) proposed a numerical scheme combining unconditional stability, second-order accuracy and numerical dissipation of higher modes. Similar improvements were also obtained with the formulation introduced by Wood et al. (1980) and a generalization of the methods presented by Hilber et al. (1977) and Wood et al. (1980), the so-called generalized-α method, was formulated by Chung and Hulbert (1993). The generalized-α method leads to second order accuracy and optimized numerical dissipation can be obtained when linear problems are analyzed. Moreover, minimal dissipation is observed in the lower modes as well as maximal dissipation is achieved in the higher modes.

The development of energy-conserving algorithms was motivated from the work presented by Belytschko and Schoeberle (1975), where a stability condition based on energy variables was proposed. Earlier investigations already indicated that algorithms presenting unconditional stability for applications in linear dynamics are subject to numerical instability when the corresponding nonlinear case is analyzed. Following the energy criterion introduced by Belytschko and Schoeberle (1975), many algorithms were presented for applications involving nonlinear dynamics, such as the energy-conserving scheme introduced by Hughes et al. (1978), where the Lagrange multiplier method is adopted to enforce energy conservation. Nevertheless, Ortiz (1986) demonstrated that energy conservation is not sufficient for maintaining numerical stability in the nonlinear range. Kuhl and Ramm (1996) also observed that the energy method presented by Hughes et al. (1978) conserves the total energy perfectly, but leads to failure in the iteration procedure related to the Newton-Raphson linearization.

Indeed, Simo and Tarnow (1992) had already noticed the importance of momentum conservation by proposing the energy-momentum method, which conserves total energy as well as linear and angular momentum. Furthermore, second-order accuracy is also preserved. The energy-momentum method was developed considering the mid-point rule to evaluate the internal forces in every time step of the time integration process in order to reach energy conservation algorithmically, since it was concluded that the stress update procedure is crucial to obtain a numerical algorithm with energy-momentum conservation. An energy-momentum conserving algorithm for hypoelastic constitutive models was developed by Noels et al. (2004) by using a new expression for evaluating the internal forces at element level. Braun and Awruch (2008) also utilized a hypoelastic formulation for applications in nonlinear elastodynamics using the eight-node hexahedral element with one-point quadrature techniques. According to Romero (2012), there are infinite ways of obtaining second order accuracy as well as energy and momentum conservation algorithms, whereas the characterization of the conserving stress as a minimization problem leads to that conclusion.

Although the conservation of energy and momentum is mandatory in order to obtain a stable numerical algorithm, it was also realized that some amount of numerical dissipation must be introduced in the model to damp out spurious contributions of the high-frequency range to the dynamic response. This situation motivated the development of energy dissipative momentum conserving algorithms, where momentum is conserved, energy dissipation is controlled and order of accuracy is maintained. Kuhl and Ramm (1996) proposed the constraint energy-momentum method, a time-stepping scheme combining conservation and dissipation properties, where energy and momentum are enforced considering the constraint energy methodology proposed by Hughes et al. (1978) and the generalized-α method (Chung and Hulbert, 1993) is utilized in order to obtain a dissipative time integration model. Optimized parameters for the α methods were determined leading to an integration procedure with less numerical dissipation for lower frequencies and more dissipation on higher frequencies of the energy spectrum. An algorithm based on controllable numerical dissipation and the energy-momentum method introduced by Simo and Tarnow (1992) was presented by Kuhl and Crisfield (1999) considering a nonlinear version of the generalized-α method. Reviews on energy-momentum and dissipative methods may be found in Khul and Crisfield (1999), Armero and Romero (2001a) and Erlicher et al. (2002).

In the present work, a numerical model based on isogeometric analysis is developed for applications in nonlinear elastodynamics. The kinematic description of the continuum is performed using the corotational approach in the context of isogeometric analysis. A hypoelastic constitutive model is adopted utilizing corotational stress and strain tensors, where the small strain hypothesis and large displacements and rotations are considered. The numerical model is obtained by applying the Bubnov-Galerkin weighted residual method on the Cauchy's equation of motion and a Newton-Raphson scheme is adopted for linearization of the residual vector in the nonlinear range. Geometry and solution fields are approximated using NURBS basis functions according to the isoparametric concept. The generalized energy-momentum method is implemented into the isogeometric formulation in order to obtain a stable and dissipative scheme for time integration. The influence of aspects related to the isogeometric discretization is investigated for numerical applications where numerical instabilities are expected when standard finite element models are utilized

2 GOVERNING EQUATIONS FOR LINEAR AND NONLINEAR ELASTODYNAMICS

Problems on elastodynamics may be formulated considering the Cauchy's equation of

motion, where mass and energy conservation must be also enforced over the volume enclosing the body analyzed (see, for instance, Malvern, 1969). Considering a classical Lagrangian kinematical description in the Cartesian coordinate system and in the absence of temperature changes, the system of governing equations are reduced to the following expressions:

$$\int_{\Omega_0} \rho\left(\mathbf{X}, t_0\right) \mathrm{d}\Omega = \int_{\Omega} \rho\left(\mathbf{x}, t\right) \mathrm{d}\Omega \tag{1}$$

$$\nabla.\boldsymbol{\sigma}(\mathbf{u}) + \rho\mathbf{b} = \rho\frac{\partial \mathbf{v}}{\partial t} \qquad \text{in } \Omega\,; t \in [t_0, t_\mathrm{f}] \tag{2}$$

$$\mathbf{u} = \bar{\mathbf{u}} \qquad \text{on } \Gamma_\mathrm{u}\ ;\ t \in [t_0, t_\mathrm{f}] \tag{3}$$

$$\boldsymbol{\sigma}.\mathbf{n} = \bar{\mathbf{t}} \qquad \text{on } \Gamma_\mathrm{f}\ ;\ t \in [t_0, t_\mathrm{f}] \tag{4}$$

$$\mathbf{u}(\mathbf{x}, t_0) = \mathbf{u}_0(\mathbf{x}) \quad ; \quad \mathbf{v} = \frac{\partial \mathbf{u}}{\partial t}(\mathbf{x}, t_0) = \dot{\mathbf{u}}_0(\mathbf{x}) \quad \mathbf{x} \in \Omega \tag{5}$$

where Eqs. (1) and (2) represent mass and momentum balances over the spatial domain $\Omega(t)$ corresponding to the body, respectively, with the vectors $\mathbf{X}$ and $\mathbf{x}$ containing components of the material (X_i) and spatial (x_i) coordinates in the Cartesian coordinate system, t denotes time, ρ is the specific mass of the body, ∇ is the differential operator, $\mathbf{b}$ is the vector of body forces per unit mass, $\boldsymbol{\sigma}$ contains components of the Cauchy stress tensor and $\mathbf{u}$ and $\mathbf{v}$ are the displacement and velocity vectors. The boundary conditions are given according to Eqs. (3) and (4), where $\bar{\mathbf{u}}$ is the vector of prescribed displacements, $\bar{\mathbf{t}}$ is the prescribed traction vector and $\mathbf{n}$ is the unit outward normal vector defined at a point on boundary Γ_f. Equation (5) specifies the initial conditions ($t = t_0$; $\Omega = \Omega_0$) for the displacement and velocity fields. The Cauchy's equation of motion (Eq. 2) is derived considering the current deformed configuration of the body (Ω), which boundary Γ is composed by the subsets Γ_u and Γ_f, such that $\Gamma = \Gamma_\mathrm{u} \cup \Gamma_\mathrm{f}$.

In the present model, geometrically nonlinear problems are analyzed taking into account the corotational approach, where stress and strain are described according to a coordinate system locally attached to every element of the computational mesh. Consequently, a linear constitutive model restricted to small strains can be adopted in order to relate strain and stress measures, which may be written as:

$$\hat{\boldsymbol{\sigma}} = \mathbf{C}\hat{\boldsymbol{\varepsilon}} = \lambda\, tr\left(\hat{\boldsymbol{\varepsilon}}\right)\mathbf{I} + 2\mu\hat{\boldsymbol{\varepsilon}} \tag{6}$$

where $\hat{\boldsymbol{\sigma}}$ and $\hat{\boldsymbol{\varepsilon}}$ are the Cauchy stress tensor and the small strain tensor, respectively, both defined in the corotational system, $\mathbf{C}$ is the fourth-order isotropic elastic tensor, which is described in terms of the Lamé constants λ and μ. It is important to notice that when infinitesimal displacements and rotations are observed, the geometrical linear approach can be utilized and the undeformed configuration of the body (Ω_0) is taken as reference throughout the numerical analysis.

Corotational formulations adopted in finite element models are usually defined considering local coordinate systems positioned at the quadrature points of the elements constituting the finite element mesh. The same procedure is employed in isogeometric analysis, taking into

account that the motion at element level is now described in terms of displacements defined at the control points. Assuming that all kinematical variables at the previous configuration t_n of the body are known, the displacement field at the end of the current time step can be obtained from integration of the strain rate tensor over the time interval defining the present time increment $[t_n,\ t_{n+1}]$. In addition, this integration to obtain the strain increment must be performed in the corotational coordinate system, where only the deformational part of the displacement increment is considered. The strain rate tensor in the corotational system is defined as follows:

$$\dot{\hat{\boldsymbol{\varepsilon}}} = \frac{1}{2}\left[\frac{\partial \hat{\mathbf{v}}^{\text{def}}}{\partial \hat{\mathbf{x}}} + \left(\frac{\partial \hat{\mathbf{v}}^{\text{def}}}{\partial \hat{\mathbf{x}}} \right)^{\text{T}} \right] \tag{7}$$

where $\hat{\mathbf{v}}^{\text{def}}$ represents the velocity field associated with the deformation part of the motion in the corotational coordinate system $\hat{\mathbf{x}}$. In order to obtain strain increments, some methodology must be adopted to integrate the strain tensor over the time interval $[t_n, t_{n+1}]$. According to the mid-point integration (see Hughes and Winget, 1980), the strain increment may be obtained from:

$$\Delta\hat{\boldsymbol{\varepsilon}} = \int_{t_n}^{t_{n+1}} \dot{\hat{\boldsymbol{\varepsilon}}}\, d\tau = \frac{1}{2}\left[\frac{\partial \Delta\hat{\mathbf{u}}^{\text{def}}}{\partial \hat{\mathbf{x}}_{n+1/2}} + \left(\frac{\partial \Delta\hat{\mathbf{u}}^{\text{def}}}{\partial \hat{\mathbf{x}}_{n+1/2}} \right)^{\text{T}} \right] \tag{8}$$

where $\Delta\hat{\mathbf{u}}^{\text{def}}$ is the deformation part of the displacement increment in the corotational system and $\hat{\mathbf{x}}_{n+1/2}$ is the intermediate configuration of the body defined in the corotational system, which can be determined according to the following expression:

$$\hat{\mathbf{x}}_{n+1/2} = \mathbf{R}_{n+1/2}\mathbf{x}_{n+1/2} = \frac{1}{2}\mathbf{R}_{n+1/2}\left(\mathbf{x}_{n+1} + \mathbf{x}_n\right) \tag{9}$$

where $\mathbf{R}_{n+1/2}$ is the orthogonal transformation matrix performing rotation from the global system to the corotational system defined locally at the intermediate configuration $t_{n+1/2}$.

The displacement increment referring to the present time interval $[t_n,\ t_{n+1}]$ can be decomposed as follows:

$$\Delta\mathbf{u} = \Delta\mathbf{u}^{\text{def}} + \Delta\mathbf{u}^{\text{rot}} \tag{10}$$

where $\Delta\mathbf{u}^{\text{def}}$ and $\Delta\mathbf{u}^{\text{rot}}$ are, respectively, the deformation and rotation parts of the displacement increment defined in the global coordinate system. It is important to notice that the decomposition described in Eq. (10) is locally performed at element level. The deformation displacement increment in the corotational system can be obtained from the following expression:

$$\Delta\hat{\mathbf{u}}^{\text{def}} = \mathbf{R}_{n+1/2}\Delta\mathbf{u}^{\text{def}} = \hat{\mathbf{x}}_{n+1} - \hat{\mathbf{x}}_n \tag{11}$$

where the transformation matrix is evaluated at the intermediate configuration $t_{n+1/2}$ of the current time interval $[t_n,\ t_{n+1}]$, since the strain rate tensor must be referred to the body configuration at $t_{n+1/2}$. Coordinates corresponding to the previous and current configurations of the body in the corotational system are obtained with following transformations:

$$\hat{\mathbf{x}}_n = \mathbf{R}_n\mathbf{x}_n; \qquad \hat{\mathbf{x}}_{n+1} = \mathbf{R}_{n+1}\mathbf{x}_{n+1} \tag{12}$$

where $\mathbf{R}_n$ and $\mathbf{R}_{n+1}$ are orthogonal transformation matrices performing rotations from the

global system to the corotational system defined locally at t_n and t_{n+1}, respectively.

A hypoelastic constitutive formulation is very effective for corotational descriptions, since the nonlinear problem can be posed in rate form by considering the small strain hypothesis and an objective rate of the Cauchy stress tensor. Consequently, after determining the strain increment in the corotational system, strain and stress updates can be performed with the following equations:

$$\begin{aligned} \hat{\boldsymbol{\varepsilon}}_{n+1} &= \hat{\boldsymbol{\varepsilon}}_n + \Delta\hat{\boldsymbol{\varepsilon}} \\ \hat{\boldsymbol{\sigma}}_{n+1} &= \hat{\boldsymbol{\sigma}}_n + \Delta\hat{\boldsymbol{\sigma}} \end{aligned} \tag{13}$$

where n and n+1 denote the previous and current configurations in the corotational system, respectively. In order to obtain an incrementally objective constitutive formulation, the Truesdell rate tensor is adopted in this work, which may be described as follows:

$$\dot{\hat{\boldsymbol{\sigma}}}^{\nabla^{TR}} = \dot{\hat{\boldsymbol{\sigma}}} - \hat{\mathbf{L}}\hat{\boldsymbol{\sigma}} - \hat{\boldsymbol{\sigma}}\hat{\mathbf{L}}^{\mathrm{T}} + \hat{\boldsymbol{\sigma}}\, tr\dot{\hat{\boldsymbol{\varepsilon}}} \tag{14}$$

where $\hat{\mathbf{L}} = \dot{\hat{\boldsymbol{\varepsilon}}} + \dot{\hat{\boldsymbol{\omega}}}$ is the spatial velocity gradient tensor defined in the corotational system. The corotational spin tensor $\dot{\hat{\boldsymbol{\omega}}}$ must be also integrated over the time interval [t_n, t_{n+1}] considering the same mid-point rule adopted in Eq. (8).

In the present work, a classical polar decomposition is utilized to obtain the orthogonal transformation matrix **R**, where spectral decomposition of the right Cauchy-Green deformation tensor **C** is adopted to obtain the right stretch tensor **U**. The right Cauchy-Green deformation tensor is defined as function of the deformation gradient tensor **F** as follows:

$$\mathbf{C} = \mathbf{F}^{\mathrm{T}}.\mathbf{F} \tag{15}$$

where the polar decomposition theorem **F** = **Q.U** is invoked in order to obtain the relation between **C** and **U**, that is:

$$\mathbf{C} = \mathbf{U}^{\mathrm{T}}.\mathbf{Q}^{\mathrm{T}}.\mathbf{Q}.\mathbf{U} = \mathbf{U}^2 \tag{16}$$

By using spectral decomposition of **C**, the following expression is obtained:

$$\mathbf{C} = \sum_{i=1} \lambda_i^2 \mathbf{N}_i \otimes \mathbf{N}_i = \mathbf{U}^2 \tag{17}$$

where λ_i and $\mathbf{N}_i$ are, respectively, the eigenvalues and the eigenvectors of **C**. Consequently, the rotation tensor **Q** can be evaluated from:

$$\mathbf{Q} = \mathbf{F}.\mathbf{U}^{-1} = \mathbf{F}.\sum_{i=1} \left(\lambda_i^{-1} \mathbf{N}_i \otimes \mathbf{N}_i \right) \tag{18}$$

The transformation matrix utilized in the corotational formulation is obtained considering that $\mathbf{R} = \mathbf{Q}^{\mathrm{T}}$.

3 THE NUMERICAL MODEL

A numerical model based on isogeometric analysis may be constructed using variational principles in the same form as that utilized by the FEM, which are equivalent to consider the corresponding weak forms obtained from the Galerkin method applied to the governing equations. In elastodynamics, the Hamilton's principle can be adopted according to the following expression:

$$\int_{t_0}^{t_f} \delta\left(K-\pi\right) dt + \int_{t_0}^{t_f} \delta W_D \, dt = 0 \tag{19}$$

with:

$$K = \frac{1}{2}\int_{\Omega} \rho \dot{\mathbf{u}}^T.\dot{\mathbf{u}} \, d\Omega \quad ; \quad \delta K = \int_{\Omega} \rho \dot{\mathbf{u}}^T.\delta\dot{\mathbf{u}} \, d\Omega \tag{20}$$

$$\begin{aligned} \pi &= \int_{\Omega} U(\boldsymbol{\varepsilon}) \, d\Omega - \int_{\Omega} \rho \mathbf{u}^T.\mathbf{b} \, d\Omega - \int_{\Gamma_f} \mathbf{u}^T.\mathbf{t} \, d\Gamma \\ \delta\pi &= \int_{\Omega} \boldsymbol{\sigma}\delta\boldsymbol{\varepsilon} \, d\Omega - \int_{\Omega} \rho\delta\mathbf{u}^T.\mathbf{b} \, d\Omega - \int_{\Gamma_f} \delta\mathbf{u}^T.\mathbf{t} \, d\Gamma \end{aligned} \tag{21}$$

$$W_D = -\int_{\Omega} \mathbf{u}^T.\mathbf{d} \, d\Omega \quad ; \quad \delta W_D = -\int_{\Omega} \delta\mathbf{u}^T.\mathbf{d} \, d\Omega \tag{22}$$

where K and π are the kinetic energy and the total potential energy, respectively, with δK and $\delta\pi$ denoting its corresponding variations, W_D is the work done by any nonconserving force of the system and δW_D is the respective variation, $U(\boldsymbol{\varepsilon}) = \int_{\boldsymbol{\varepsilon}_0}^{\boldsymbol{\varepsilon}} \boldsymbol{\sigma} \, d\boldsymbol{\varepsilon}$ is the strain energy density function and $\mathbf{d}$ is the vector of nonconserving forces, including damping. The displacement variations $\delta\mathbf{u}$ must vanish at the time limits t_0 and t_f and also on boundary Γ_u, where displacements are imposed.

The semidiscrete system of momentum equations is obtained taking into account they are discrete in space but continuous in time. The space discretization is performed here considering the Bubnov-Galerkin method applied into the context of isogeometric analysis, where the displacement variations associated with the variational form (see Eq. 19) assume the role of weight functions. By integrating by parts the kinetic energy variation presented in Eq. (19) and considering the restrictions imposed on the displacement variations $\delta\mathbf{u}$ at the time limits t_0 and t_f, the following expression is obtained:

$$\int_{\Omega} \delta\mathbf{u}^T \rho\ddot{\mathbf{u}} \, d\Omega + \int_{\Omega} \delta\mathbf{u}^T\mathbf{d} \, d\Omega + \int_{\Omega} (\nabla\delta\mathbf{u})^T \boldsymbol{\sigma} \, d\Omega = \int_{\Omega} \delta\mathbf{u}^T \rho\mathbf{b} \, d\Omega + \int_{\Gamma} \delta\mathbf{u}^T\mathbf{t} \, d\Gamma \tag{23}$$

where the time integrals were omitted for the sake of clarity.

3.1 Spatial discretization – the isogeometric formulation using NURBS

In order to define the element concept in the context of isogeometric analysis, geometry, displacements and displacement variations must be discretized with the following expressions:

$$\begin{aligned} &\mathbf{x}(\xi,\eta,\zeta,t) = \sum_{a=1}^{n_{cp}} R_a(\xi,\eta,\zeta)\,\mathbf{x}_a(t); \qquad \mathbf{u}(\xi,\eta,\zeta,t) = \sum_{a=1}^{n_{cp}} R_a(\xi,\eta,\zeta)\,\mathbf{u}_a(t); \\ &\delta\mathbf{u}(\xi,\eta,\zeta,t) = \sum_{a=1}^{n_{cp}} R_a(\xi,\eta,\zeta)\,\delta\mathbf{u}_a(t) \end{aligned} \tag{24}$$

where R_a is the NURBS basis function related to control point a, which is defined as function of the parametric coordinates (ξ,η,ζ), and n_{cp} is the number of global control points. Knot

vectors corresponding to the different directions in the parametric space must be also specified defining the non-zero knot spans where elements are then identified. A three-dimensional knot vector (Ξ, Λ, Ψ) may be written as follows:

$$\begin{aligned}\Xi(\boldsymbol{\xi}) &= \left\{ \underbrace{0,\ldots,0}_{p+1}, \xi_{p+1},\ldots,\xi_{s_p-p-1}, \underbrace{1,\ldots,1}_{p+1} \right\} \\ \Lambda(\boldsymbol{\eta}) &= \left\{ \underbrace{0,\ldots,0}_{q+1}, \eta_{q+1},\ldots,\eta_{s_q-q-1}, \underbrace{1,\ldots,1}_{q+1} \right\} \\ \Psi(\boldsymbol{\zeta}) &= \left\{ \underbrace{0,\ldots,0}_{r+1}, \zeta_{r+1},\ldots,\zeta_{s_r-r-1}, \underbrace{1,\ldots,1}_{r+1} \right\}\end{aligned} \tag{25}$$

with $s_\mathrm{p} = n + p + 1$, $s_\mathrm{q} = m + q + 1$ and $s_\mathrm{r} = l + r + 1$, where p, q and r are the polynomial degrees of the basis functions over the parametric directions ξ, η and ζ, respectively, and the corresponding numbers of basis functions are specified by $n + 1$, $m + 1$ and $l + 1$, respectively, which are also associated with the number of control points in the different directions of the physical space. Depending on the geometric topology of the problem, the knot vector may be reduced to two- or one-dimensional vectors, i.e. (Ξ, Λ) and (Ξ).

The NURBS basis functions for three-dimensional applications are defined by:

$$R_{i,j,k}^{p,q,r}(\xi,\eta,\zeta) = \frac{N_{i,p}(\xi)N_{j,q}(\eta)N_{k,r}(\eta)w_{i,j,k}}{\sum_{\hat{i}=0}^{n}\sum_{\hat{j}=0}^{m}\sum_{\hat{k}=0}^{l} N_{\hat{i},p}(\xi)N_{\hat{j},q}(\eta)N_{\hat{k},r}(\eta)w_{\hat{i},\hat{j},\hat{k}}} \tag{26}$$

where the subscripts i, j and k indicate the position of the control point in the index space and the superscripts p, q and r define the polynomial degree of the basis functions. The weight term $w_{i,j,k}$ is related to the weight associated with the control point defined by the subindices i, j and k, considering that if the weights are specified with unit values, then $R_i^p = N_{i,p}$. Details on evaluation of weight functions may be found in Piegl and Tiller (1997) and Cotrell et al. (2009). For one- and two-dimensional problems, the following NURBS functions are utilized:

$$R_i^p(\xi) = \frac{N_{i,p}(\xi)w_i}{\sum_{j=0}^{n} N_{j,p}(\xi)w_j} \tag{27}$$

$$R_{i,j}^{p,q}(\xi,\eta) = \frac{N_{i,p}(\xi)N_{j,q}(\eta)w_{i,j}}{\sum_{\hat{i}=0}^{n}\sum_{\hat{j}=0}^{m} N_{\hat{i},p}(\xi)N_{\hat{j},q}(\eta)w_{\hat{i},\hat{j}}} \tag{28}$$

The Cox-de Boor recursive formulation (Cox, 1971; De Boor, 1972) is usually adopted to evaluate B-spline basis functions, which are obtained considering a given one-dimensional knot vector Ξ ($\boldsymbol{\xi}$) defined over the parametric space ξ, the number of control points defined along the corresponding direction in the physical space and the polynomial order of the corresponding basis functions. According to the Cox-de Boor formulation, the B-spline basis functions may be expressed as:

$$N_{i,p}(\xi) = \frac{\xi - \xi_i}{\xi_{i+p} - \xi_i} N_{i,p-1}(\xi) + \frac{\xi_{i+p+1} - \xi}{\xi_{i+p+1} - \xi_{i+1}} N_{i+1,p-1}(\xi) \tag{29}$$

where p is the polynomial degree of the basis function $N(\xi)$, which is valid for $p \geq 1$, and i is the knot index. The recursion is performed over the polynomial degree until $p = 0$, when the following equation is utilized:

$$N_{i,0}(\xi) = \begin{cases} 1 & \text{for } \xi_i \leq \xi < \xi_{i+1} \\ 0 & \text{otherwise} \end{cases} \tag{30}$$

Equations (29) and (30) are straightforwardly extended to the basis functions associated with the parametric directions η and ζ. For additional information on the isogeometric formulation utilized in this work see Espath et al. (2011).

The isogeometric model for the equation of motion given by Eq. (23) can be written as:

$$\sum_{e=1}^{n_{el}} \left(\int_{\Omega_e} \delta \mathbf{u}^{\mathrm{t}} \rho \ddot{\mathbf{u}} \, \mathrm{d}\Omega_e \right) + \sum_{e=1}^{n_{el}} \left(\int_{\Omega_e} (\nabla \delta \mathbf{u})^{\mathrm{T}} \boldsymbol{\sigma} \, \mathrm{d}\Omega_e \right) = \sum_{e=1}^{n_{el}} \left(\int_{\Omega_e} \delta \mathbf{u}^{\mathrm{T}} \mathbf{b} \, \mathrm{d}\Omega_e + \int_{\Gamma_e} \delta \mathbf{u}^{\mathrm{T}} \mathbf{t} \, \mathrm{d}\Gamma_e \right) \tag{31}$$

where Ω_e and Γ_e are, respectively, volume and boundary surface corresponding to element e in the physical mesh. Considering $n + 1$, $m + 1$ and $l + 1$ as the number of basis functions related to the parametric directions ξ, η and ζ, respectively, and their respective polynomial degrees denoted by p, q and r, element e is defined by determining the indices at which the corresponding non-zero knot span begins in the index space, that is:

$$e \in \left[\xi_i, \xi_{i+1}\right] \times \left[\eta_j, \eta_{j+1}\right] \times \left[\zeta_k, \zeta_{k+1}\right] \tag{32}$$

where $p+1 \leq i \leq n$, $q+1 \leq j \leq m$ and $r+1 \leq k \leq l$ (see Eq. 25). The total number of elements in which the spatial field is discretized in the parametric domain is defined as:

$$n_{el} = (n - p + 1)(m - q + 1)(l - r + 1) \tag{33}$$

By substituting the NURBS approximation related to the displacement field (see Eq. 24) into the constitutive equation (see Eq. 6), an element level approximation of the stress-strain relation is obtained, where the strain components in the corotational system are given by:

$$\hat{\boldsymbol{\varepsilon}} = \hat{\mathbf{B}} \hat{\mathbf{u}} \tag{34}$$

where $\hat{\mathbf{B}}$ and $\hat{\mathbf{u}}$ are the gradient matrix and the displacement vector, which are evaluated referring to the current configuration of the body in the corotational coordinate system. When infinitesimal displacements and rotations are observed, Eq. (34) is described in terms of the undeformed configuration of the body (Ω_0). Derivatives of the B-spline basis functions are represented in terms of B-spline lower order bases owing to the recursive definition of the basis functions. Algorithms for numerical evaluation of derivatives of B-spline basis functions may be found in Piegl and Tiller (1997).

Introducing the expansions shown in Eq. (24) and the relationship given by Eq. (34) into Eq. (31), a matrix equation representing a system of algebraic equations is obtained for the equation of motion, which may be expressed as:

$$\sum_{e=1}^{n_{el}} \mathbf{M}^{\mathbf{e}} \ddot{\mathbf{u}} + \sum_{e=1}^{n_{el}} \mathbf{K}^{\mathbf{e}} \mathbf{u} = \sum_{e=1}^{n_{el}} \mathbf{f}^{\mathbf{e}} \tag{35}$$

where $\mathbf{M}^{\mathbf{e}}$ and $\mathbf{K}^{\mathbf{e}}$ are the element mass and element stiffness matrices, respectively, and $\mathbf{f}^{\mathbf{e}}$ is

the force vector at element level. The matrix and vector dimensions associated with $\mathbf{M}^{\mathbf{e}}$ and $\mathbf{K}^{\mathbf{e}}$, and $\mathbf{f}^{\mathbf{e}}$, are specified as $(n_{eq}.n_{eq}.n_{eq})$ and (n_{eq}), respectively, where $n_{eq} = n_{en}.n_{df}$, with n_{df} denoting the number of degrees of freedom at the control point level. The summation symbol indicates the assembling procedure to evaluate the global system of equations, considering the element contributions given according to connectivity relations established among the control points. The global stiffness matrix is always sparse because the support of each basis function is highly localized.

In the geometrically nonlinear regime, the system of equations represented by Eq. (35) must be iteratively satisfied using the incremental approach (see Bathe, 1996), since internal forces are given now as functions of the current configuration of the body. The nonlinear equation of motion is obtained employing a linearization procedure given by the Newton-Raphson method, where the residual vector is submitted to a Taylor series expansion within the increment interval $[t_{\mathrm{n}}, t_{\mathrm{n+1}}]$. Consequently, Eq. (35) must be rewritten as follows:

$$\sum_{e=1}^{nel} \mathbf{M}^{\mathbf{e}}\ddot{\mathbf{u}} + \sum_{e=1}^{nel} \mathbf{K}_{\mathbf{tan}}^{\mathbf{e}}\left(\mathbf{u}^{\mathbf{e}}\right)\Delta\mathbf{u} = \sum_{e=1}^{nel} \mathbf{f}^{\mathbf{e}} - \sum_{e=1}^{nel} \mathbf{f}_{\mathbf{int}}^{\mathbf{e}}\left(\mathbf{u}^{\mathbf{e}}\right) \tag{36}$$

where $\mathbf{K}_{\mathrm{tan}}$ is the tangent stiffness matrix. At each iterative step, the tangent stiffness matrix and the internal force vector are initially evaluated in the corotational coordinate system with the following expressions:

$$\hat{\mathbf{K}}_{\mathbf{tan}}^{\mathbf{e}} = \int_{\hat{\Omega}_e} \mathbf{B}^{\mathrm{T}}(\mathbf{C} + \hat{\mathbf{D}})\mathbf{B}\, \mathrm{d}\hat{\Omega}_e; \qquad \hat{\mathbf{f}}_{\mathbf{int}}^{\mathbf{e}} = \int_{\hat{\Omega}_e} \mathbf{B}^{\mathrm{T}}\hat{\boldsymbol{\sigma}}\, \mathrm{d}\hat{\Omega}_e \tag{37}$$

where $\hat{\Omega}_e$ is referred to the current configuration of element e in the corotational coordinate system, $\hat{\mathbf{D}}$ and $\hat{\boldsymbol{\sigma}}$ are stress tensors related to the Truesdell rate tensor and the corotational Cauchy stress tensor, respectively, with both evaluated in the corotational coordinate system. See Duarte Filho and Awruch (2004) and Braun and Awruch (2008) for further details.

In order to solve the system of nonlinear equations, the tangent stiffness matrix and the internal force vector must be obtained in the global coordinate system through objective transformation from the corotational system, that is:

$$\mathbf{K}_{\mathbf{tan}}^{\mathbf{e}} = \mathbf{R}^{\mathrm{T}}\hat{\mathbf{K}}_{\mathbf{tan}}^{\mathbf{e}}\mathbf{R}; \qquad \mathbf{f}_{\mathbf{int}}^{\mathbf{e}} = \mathbf{R}^{\mathrm{T}}\hat{\mathbf{f}}_{\mathbf{int}}^{\mathbf{e}} \tag{38}$$

where $\mathbf{R}$ is the transformation matrix defined in the previous section.

When a numerical model based on isogeometric analysis is formulated with the Galerkin method and NURBS basis functions, homogeneous boundary conditions are exactly enforced by setting the corresponding control variables as zero. A trivial procedure for imposition of essential boundary conditions is then obtained, which is similar to that utilized by finite element models. In the present model, the Kroenecker delta property of the NURBS basis functions can be applied on the displacement field as follows:

$$\mathbf{u}(\mathbf{x}_B) = \sum_{A=1}^{ncp} R_A(\xi_B, \eta_B, \zeta_B)\,\mathbf{u}_A = 0 \qquad \text{with} \qquad R_A(\mathbf{x}_B) = \delta_{AB} \tag{39}$$

where vector $\mathbf{x}_B$ specifies Cartesian coordinates of control points with parametric coordinates defined by ξ_B, η_B and ζ_B, which are located at boundary knots with essential boundary conditions.

3.2 Temporal discretization – the generalized energy-momentum method

The time interval during which the dynamic analysis is carried out $[t_0, t_f]$ is subdivided into time steps $\Delta t = t_{n+1} - t_n$ in order to define the time discretization process for implicit algorithms, where the incremental approach is adopted. The kinematic variables are assumed to be known at the beginning of every time step of the time integration and the same variables are obtained at the end of the respective time step considering the solution of the equation of motion, which is given in terms of displacement increments, and time approximations provided by a specific method, such as the Newmark's method. Although the Newmark's algorithm is unconditionally stable for linear problems, it may be unstable in the nonlinear range. In this sense, the generalized-α method may be utilized, where the equilibrium of the equation of motion is verified at some intermediate point of the time increment instead of the end point employed by the classical Newmark scheme. The kinematic variables are defined in the generalized-α method by using the following functions:

$$\begin{aligned} \ddot{\mathbf{u}}_{n+1-\alpha_m} &= (1-\alpha_m)\,\ddot{\mathbf{u}}_{n+1} + \alpha_m \ddot{\mathbf{u}}_n \\ \dot{\mathbf{u}}_{n+1-\alpha_f} &= (1-\alpha_f)\,\dot{\mathbf{u}}_{n+1} + \alpha_f \dot{\mathbf{u}}_n \\ \mathbf{u}_{n+1-\alpha_f} &= (1-\alpha_f)\,\mathbf{u}_{n+1} + \alpha_f \mathbf{u}_n \end{aligned} \tag{40}$$

with subscripts denoting time positions within the time interval $[t_n, t_{n+1}]$ as functions of the time integration parameters α_m and α_f, where n and $n+1$ correspond to initial and end points of the time interval Δt, respectively.

Introducing Newmark approximations for $\dot{\mathbf{u}}_{n+1}$ and $\ddot{\mathbf{u}}_{n+1}$ (see, for instance, Bathe, 1996) into the expressions given by Eq. (40), the number of unknowns is reduced to the displacement vector $\mathbf{u}_{n+1}$, as it is demonstrated below:

$$\dot{\mathbf{u}}_{n+1-\alpha_f} = \frac{(1-\alpha_f)\delta}{\alpha\Delta t}\left(\mathbf{u}_{n+1} - \mathbf{u}_n\right) - \frac{(1-\alpha_f)\delta - \alpha}{\alpha}\dot{\mathbf{u}}_n - \frac{(\delta - 2\alpha)(1-\alpha_f)}{2\alpha}\Delta t\ddot{\mathbf{u}}_n \tag{41}$$

$$\ddot{\mathbf{u}}_{n+1-\alpha_m} = \frac{1-\alpha_m}{\alpha\Delta t^2}\left(\mathbf{u}_{n+1} - \mathbf{u}_n\right) - \frac{1-\alpha_m}{\alpha\Delta t}\dot{\mathbf{u}}_n - \frac{1-\alpha_m - 2\alpha}{2\alpha}\ddot{\mathbf{u}}_n \tag{42}$$

where α and δ are time integration parameters specified by the Newmark's method.

However, it is well known that the generalized-α method cannot maintain numerical stability, whereas the total energy within each time step of the time integration is not controlled. In order to satisfy the stability condition, the ideas proposed by Simo and Tarnow (1992) are included in the present formulation by considering the generalized energy momentum method presented by Kuhl and Crisfield (1999). Consequently, the corotational stress tensor utilized in the internal force vector (see Eq. 37) is substituted by the algorithmic stress tensor defined in the corotational system, i.e.:

$$\hat{\boldsymbol{\sigma}}(\mathbf{u}_{n+1-\alpha_f+\nu}) = (1-\alpha_f+\nu)\hat{\boldsymbol{\sigma}}(\mathbf{u}_{n+1}) + (\alpha_f - \nu)\hat{\boldsymbol{\sigma}}(\mathbf{u}_n) \tag{43}$$

where ν denotes a numerical damping parameter, which is also considered in the algorithmic stress to introduce numerical dissipation according to the formulation presented by Armero and Petocz (1998). Moreover, the internal and external force vectors are approximated by the following expressions:

$$\mathbf{f}^{\text{ext}}_{\text{n+1-}\alpha_\text{f}} = \left(1-\alpha_\text{f}\right)\mathbf{f}^{\text{ext}}_{\text{n+1}} + \alpha_\text{f}\mathbf{f}^{\text{ext}}_{\text{n}}$$
$$\mathbf{f}^{\text{int}}_{\text{n+1-}\alpha_\text{f}} = \left(1-\alpha_\text{f}\right)\mathbf{f}^{\text{int}}_{\text{n+1}} + \alpha_\text{f}\mathbf{f}^{\text{int}}_{\text{n}} = \left(1-\alpha_\text{f}\right)\mathbf{f}^{\text{int}}(\mathbf{u}_{\text{n+1}}) + \alpha_\text{f}\mathbf{f}^{\text{int}}(\mathbf{u}_{\text{n}}) \tag{44}$$

The modified equation of motion, including damping effects, is finally presented as follows (see, for instance, Khul and Crisfield, 1999):

$$\mathbf{M}\ddot{\mathbf{u}}_{\text{n+1-}\alpha_\text{m}} + \mathbf{D}\dot{\mathbf{u}}_{\text{n+1-}\alpha_\text{f}} + \mathbf{f}^{\text{int}}_{\text{n+1-}\alpha_\text{f}} = \mathbf{f}^{\text{ext}}_{\text{n+1-}\alpha_\text{f}} \tag{45}$$

Substituting Eqs. (41) and (42) into the modified equation of motion (Eq. 45), the effective dynamic equation can be obtained, i.e.:

$$\left\{\left[\frac{1-\alpha_\text{m}}{\alpha\Delta t^2}\right]\mathbf{M} + \left[\frac{(1-\alpha_\text{f})\delta}{\alpha\Delta t}\right]\mathbf{D} + \mathbf{K}^{\text{tang}}_{\text{n+1-}\alpha_\text{f}}\right\}\Delta\mathbf{u} =$$
$$\mathbf{f}^{\text{ext}}_{\text{n+1-}\alpha_\text{f}} - \mathbf{f}^{\text{int}}_{\text{n+1-}\alpha_\text{f}}\left(\mathbf{u}^{\text{k}}_{\text{n+1}}\right) - \mathbf{M}\left[\frac{1-\alpha_\text{m}}{\alpha\Delta t}\dot{\mathbf{u}}_\text{n} + \frac{1-\alpha_\text{m}-2\alpha}{2\alpha}\ddot{\mathbf{u}}_\text{n}\right] - \tag{46}$$
$$\mathbf{D}\left\{\frac{(1-\alpha_\text{f})\delta-\alpha}{\alpha}\dot{\mathbf{u}}_\text{n} + \frac{(\delta-2\alpha)(1-\alpha_\text{f})}{2\alpha}\Delta t\ddot{\mathbf{u}}_\text{n}\right\}$$

where:

$$\mathbf{K}^{\text{tang}}_{\text{n+1-}\alpha_\text{f}} = (1-\alpha_\text{f})\mathbf{K}^{\text{tang}}(\mathbf{u}^{\text{k}}_{\text{n+1}}) \tag{47}$$

The time integration parameters α, δ, α_m and α_f are defined as functions of the spectral radius r_∞ ($0 \le \text{r}_\infty \le 1$) according to:

$$\alpha = \frac{1}{4}\left(1-\alpha_\text{m}+\alpha_\text{f}\right)^2 \quad ; \quad \delta = \frac{1}{2} - \alpha_\text{m} + \alpha_\text{f} \quad ; \quad \alpha_\text{m} = \frac{2\text{r}_\infty - 1}{\text{r}_\infty + 1} \quad ; \quad \alpha_\text{f} = \frac{\text{r}_\infty}{\text{r}_\infty + 1} \tag{48}$$

where the expressions presented above are obtained considering the formulation presented by Chung and Hulbert (1993), which leads to optimized dissipation for high and low frequencies as well as second order accuracy.

An algorithm referring to the numerical model proposed in this work is presented in Table 1, where TOL is identified as a tolerance criterion and a_0, a_1, a_2, a_3, a_4 and a_5 are constants of the generalized-α method, which are obtained from the time integration parameters α, δ, α_m and α_f defined in Eq. (48).

1. Specify the spectral radius r_∞ ($0 \le \text{r}_\infty \le 1$) and the time increment Δt.
2. Compute the time integration parameters α, δ, α_m and α_f
3. Compute the time integration constants a_0, a_1, a_2, a_3, a_4 and a_5:

$$\text{a}_0 = \frac{1-\alpha_\text{m}}{\alpha\Delta t^2}; \quad \text{a}_1 = \frac{(1-\alpha_\text{f})\delta}{\alpha\Delta t}; \quad \text{a}_2 = \frac{1-\alpha_\text{m}}{\alpha\Delta t}$$
$$\text{a}_3 = \frac{1-\alpha_\text{m}-2\alpha}{2\alpha}; \quad \text{a}_4 = \frac{(1-\alpha_\text{f})\delta-\alpha}{\alpha}; \quad \text{a}_5 = \frac{(\delta-2\alpha)(1-\alpha_\text{f})}{2\alpha}\Delta t$$

4. Solve:

$$\Delta\mathbf{u} = \left[\bar{\mathbf{K}}^{-1}\right]^{\text{t}}\bar{\mathbf{f}}^{\text{t+}\Delta\text{t}}$$

with: $$\bar{\mathbf{K}}^{t} = \mathbf{K}^{t} + a_0\mathbf{M} + a_1\mathbf{D}$$

and: $$\bar{\mathbf{f}}^{t+\Delta t} = \mathbf{f}^{ext,t+\Delta t} - \left[\mathbf{M}\ddot{\mathbf{u}} + \mathbf{D}\dot{\mathbf{u}} + \mathbf{f}^{int}(\mathbf{u})\right]^{t} + \mathbf{M}(a_2\dot{\mathbf{u}} + a_3\ddot{\mathbf{u}})^{t} + \mathbf{D}(a_4\dot{\mathbf{u}} + a_5\ddot{\mathbf{u}})^{t}$$

5. Update the displacement, velocity and acceleration vectors using Newmark approximations (see, for instance, Bathe, 1996).
6. Compute the residual load vector:

$$\mathbf{Q}^{t+\Delta t} = \mathbf{f}^{ext,t+\Delta t} - \left[\mathbf{M}\ddot{\mathbf{u}} + \mathbf{D}\dot{\mathbf{u}} + \mathbf{f}^{int}(\mathbf{u})\right]^{t+\Delta t}$$

7. Check convergence: if $\left\|\mathbf{Q}^{t+\Delta t}\right\| / \left\|\mathbf{f}^{ext,t+\Delta t}\right\| \leq \text{TOL}$ go to the next time step (4), else go to (8).
8. Compute:

$$\delta\mathbf{u} = \left[\bar{\mathbf{K}}^{-1}\right]^{t}\mathbf{Q}^{t+\Delta t}$$

9. Update the displacement, velocity and acceleration vectors using:

$$\begin{cases} \ddot{\mathbf{u}}^{k+1}_{t+\Delta t} = \ddot{\mathbf{u}}^{k}_{t+\Delta t} + a_0\delta\mathbf{u} \\ \dot{\mathbf{u}}^{k+1}_{t+\Delta t} = \dot{\mathbf{u}}^{k}_{t+\Delta t} + a_1\delta\mathbf{u} \\ \mathbf{u}^{k+1}_{t+\Delta t} = \mathbf{u}^{k}_{t+\Delta t} + \delta\mathbf{u} \end{cases}$$

10. Compute the residual load vector (step 6) with the new state of motion.
11. Check convergence: if $\left\|\mathbf{Q}^{t+\Delta t}\right\| / \left\|\mathbf{f}^{ext,t+\Delta t}\right\| \leq \text{TOL}$ go to the next time step (step 4), else go to step 8.

Table 1. Numerical algorithm for the model proposed in this work.

4 NUMERICAL APPLICATIONS

4.1 Cantilever beam

A two-dimensional cantilever beam subject to pressure loading and undergoing large displacements is analyzed in this example, where plane strain state is also assumed. Geometrical and load description for the present simulation are shown in Fig. 1 and material properties of the structure as well as the time step adopted in the time integration procedure are found in Table 2. Information on computational parameters utilized in the set of numerical analyses carried out here, which correspond to the isogeometric formulation and the time discretization scheme proposed in this work, are summarized in Table 3. Number and distribution (Lxhxz) of elements over the physical space referring to the cantilever beam are given according to the continuity class, where the element configurations (16x1x1), (21x1x1), (31x1x1) and (61x1x1) correspond to the continuity classes C^1, C^2, C^3 and C^4, respectively. The energy variables are evaluated here utilizing the following expressions:

$$\mathbf{J} = \left\{J_x \quad J_y \quad J_z\right\} = \sum_{\Omega_e=1}^{nel} \int_{V_e} \rho\mathbf{x} \otimes \dot{\mathbf{x}}\, d\Omega_e \tag{49}$$

$$E_{kin} = \sum_{\Omega_e=1}^{nel} \frac{1}{2} \int_{V_e} \rho \dot{\mathbf{x}} \cdot \dot{\mathbf{x}} \, d\Omega_e ; \qquad E_{pot} = \sum_{\Omega_e=1}^{nel} \int_{V_e} \boldsymbol{\sigma} : \boldsymbol{\varepsilon} \, d\Omega_e \tag{50}$$

where E_{pot}, E_{kin} and E_{tot} are the strain, kinetic and total energies, respectively, W_{ext} is the work done by external forces, J_x is angular momentum around x axis, J_y is angular momentum around y axis and J_z is angular momentum around z axis. The symbols (:), (.) and ($\otimes$) denote tensor, scalar and vector products, respectively. The vectors $\mathbf{x}$ and $\dot{\mathbf{x}}$ are the position vector in global coordinates and its respective time derivative, *nel* is the total number of elements, Ω_e is the element volume and $\boldsymbol{\sigma}$ and $\boldsymbol{\varepsilon}$ are stress and strain energetically conjugated tensors.

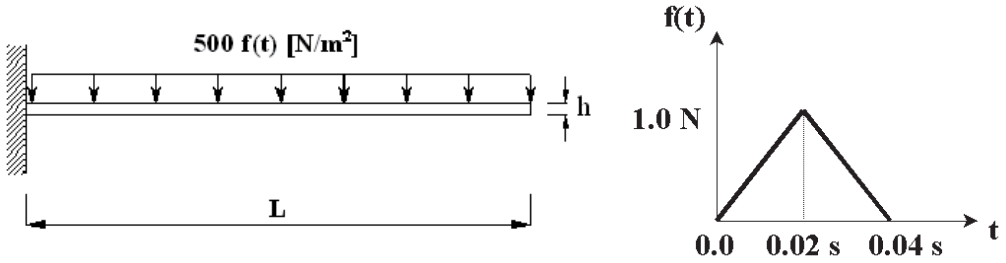

L = 0.4 m; h = 0.001 m

Figure 1. Geometrical and load characteristics for the cantilever beam analysis.

Young modulus – E [N/m^2]	7x10^{10}
Poisson coefficient – ν	0.33
Specific mass – ρ [Kg/m^3]	2.7x10^3
Damping coefficient – φ	0.0
Time step – Δt [s]	4.0x10^{-3}

Table 2. Material properties and time step utilized in the cantilever beam analysis.

Control mesh (Lxhxz)	Continuity class	Spectral radius - r_∞	Polinomial degrees (p, q, r)
66x3x2	C^1	0.95; 0.99; 1.00	5, 2, 1
66x3x2	C^2	0.95; 0.99; 1.00	5, 2, 1
66x3x2	C^3	0.95; 0.99; 1.00	5, 2, 1
66x3x2	C^4	0.95; 0.99; 1.00	5, 2, 1

Table 3. Computational parameters employed in the cantilever beam analysis.

The dynamic responses obtained from the numerical analyses performed here are shown in Figs. 2 and 3, which correspond to results presented in terms of vertical displacements evaluated at the tip of the cantilever beam during the numerical simulation and time histories referring to the respective energy variables. The present results demonstrate that the time integration process is suddenly interrupted when the amount of numerical dissipation is insufficient ($r_\infty = 0.99$) or inexistent ($r_\infty = 1.00$), unlike the finite element predictions obtained by Braun and Awruch (2008), where numerical instabilities are clearly identified from the typical increase observed in the energy response. It is important to notice that Braun and Awruch (2008) adopted a finite element formulation for eight-node hexahedral elements with one-point quadrature techniques. By increasing the continuity class, one can see that the interruption of the time integration procedure is postponed. It is also observed that the range of spectral radii with stable responses is significantly enlarged when results obtained considering the isogeometric formulation proposed in this work are compared with those

obtained by Braun and Awruch (2008) ($r_\infty \leq 0.3$). The displacement responses referring to r_∞ = 095 are in agreement with numerical predictions presented by Bathe and Baig (2005). In addition, excessive dissipation is not observed, since the total energy of the system is perfectly conserved.

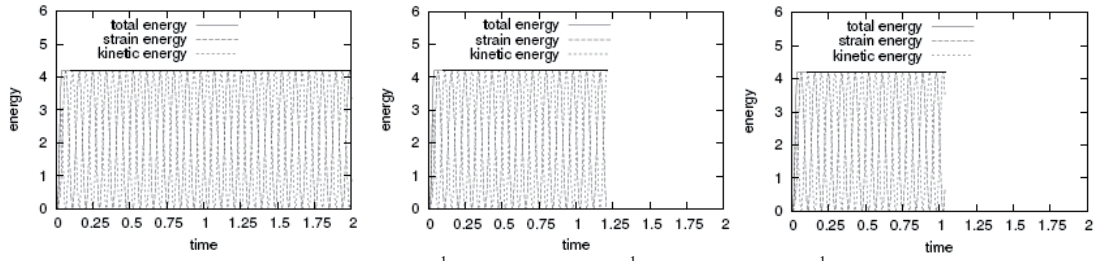

$r_\infty = 0.95$ and C^1; $r_\infty = 0.99$ and C^1; $r_\infty = 1.00$ and C^1

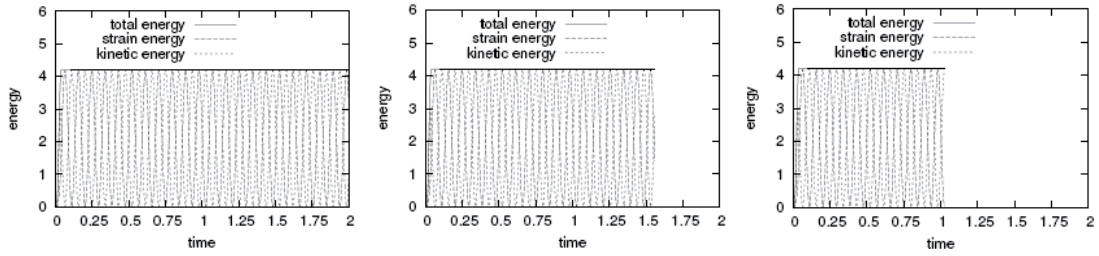

$r_\infty = 0.95$ and C^2; $r_\infty = 0.99$ and C^2; $r_\infty = 1.00$ and C^2

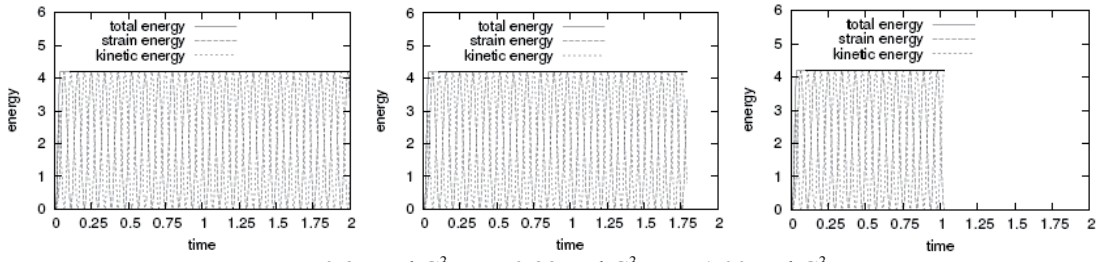

$r_\infty = 0.95$ and C^3; $r_\infty = 0.99$ and C^3; $r_\infty = 1.00$ and C^3

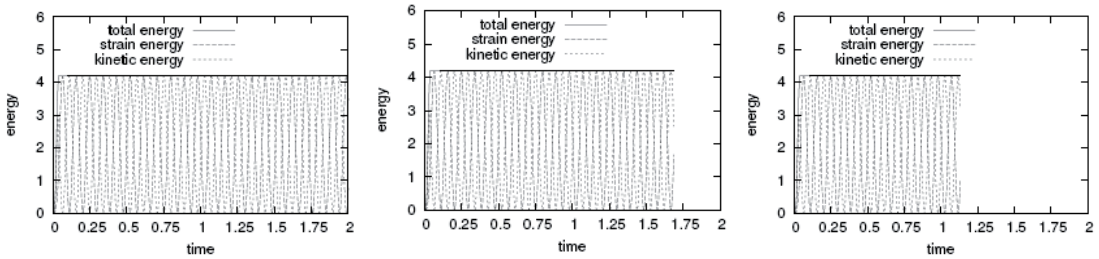

$r_\infty = 0.95$ and C^4; $r_\infty = 0.99$ and C^4; $r_\infty = 1.00$ and C^4

Figure 2. Energy responses of the cantilever beam given as function of the spectral radius (r_∞) and continuity class (C^n).

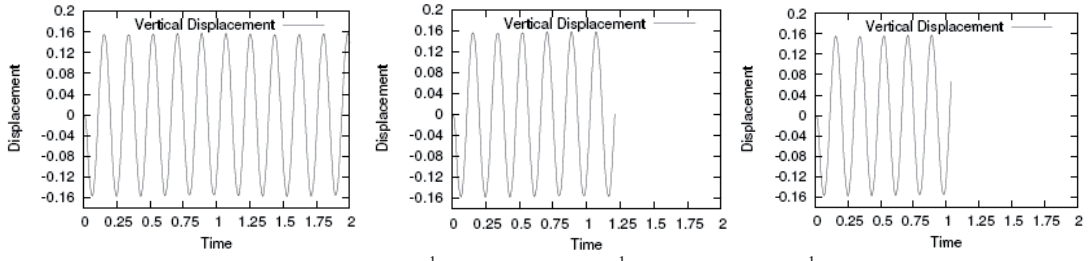

$r_\infty = 0.95$ and C^1; $r_\infty = 0.99$ and C^1; $r_\infty = 1.00$ and C^1

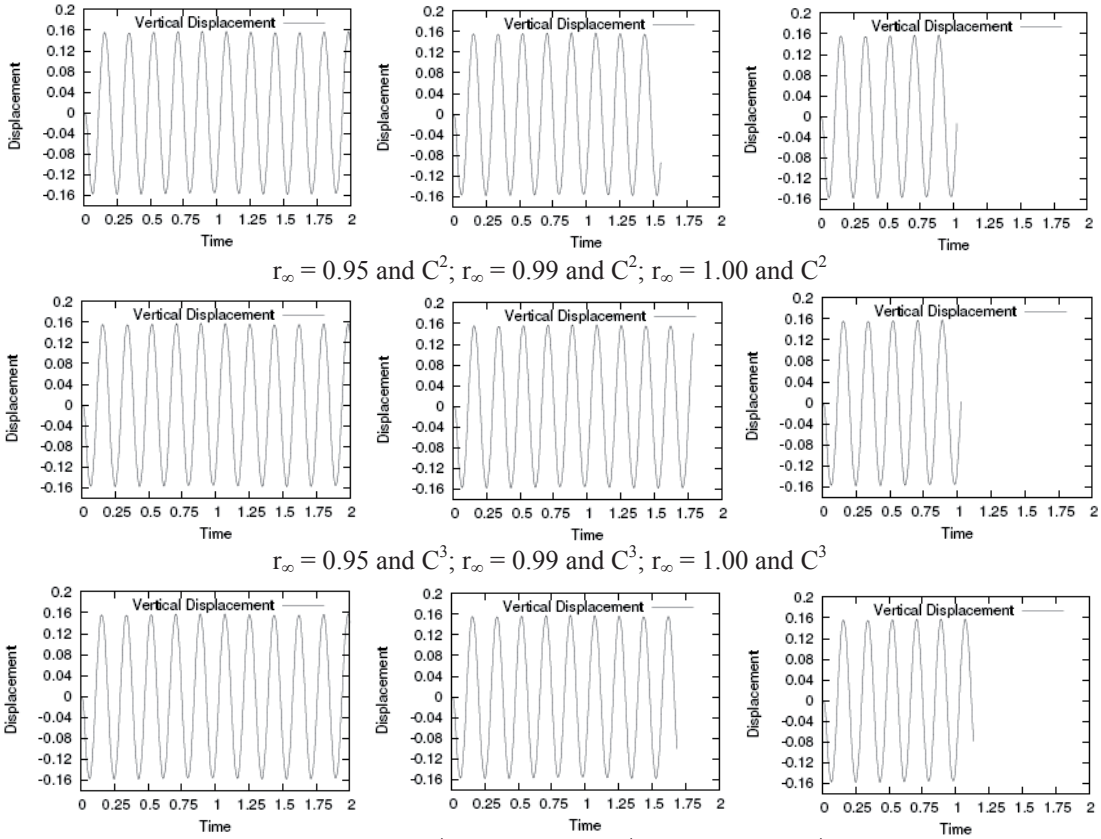

$r_\infty = 0.95$ and C^2; $r_\infty = 0.99$ and C^2; $r_\infty = 1.00$ and C^2

$r_\infty = 0.95$ and C^3; $r_\infty = 0.99$ and C^3; $r_\infty = 1.00$ and C^3

$r_\infty = 0.95$and C^4; $r_\infty = 0.99$ and C^4; $r_\infty = 1.00$ and C^4

Figure 3. Displacement responses of the cantilever beam given as function of the spectral radius (r_∞) and continuity class (C^n).

The motion of the cantilever beam during the period of oscillation [0.07s, 0.15s] can be visualized in Fig. 4, where the highly nonlinear behavior of the present application is evidenced.

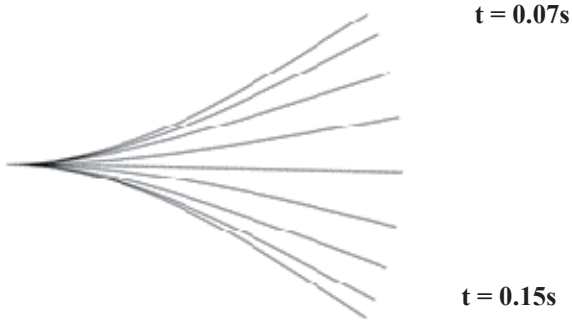

Figure 4. Deformed configurations of the beam during the time interval [0.07s, 0.15s].

4.2 Toss rule

A numerical investigation of the plane movement of a toss rule is performed in this example, where a geometrically nonlinear dynamic analysis is carried out. Geometry and load information for the present application are described in Fig. 5 and material properties of the structure as well as the time step adopted in the time integration procedure are presented in

Table 4. It is important to notice that distributed loads are applied to the structure to produce the plane motion of the rule, which is free to fly in the absence of displacement restrictions and gravity action. Computational parameters regarding the numerical analyses performed here are presented in Table 5. Number and distribution (Lxhxz) of elements over the physical space referring to the cantilever beam are again given according to the continuity class, where the element configurations (16x1x1), (21x1x1), (31x1x1) and (61x1x1) correspond to the continuity classes C^1, C^2, C^3 and C^4, respectively.

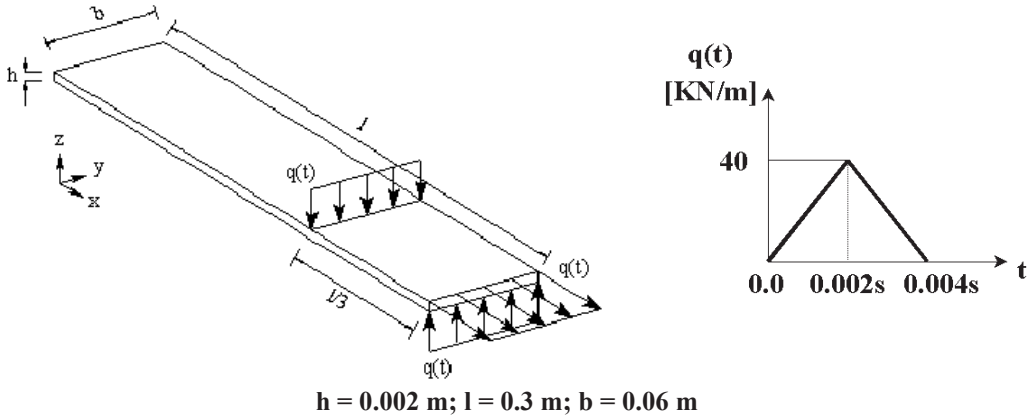

Figure 5. Geometrical and load characteristics for the toss rule analysis.

Young modulus – E [N/m^2]	2.06x10^{11}
Poisson coefficient – ν	0.3
Specific mass – ρ [Kg/m^3]	7.8x10^3
Damping coefficient – φ	0.0
Time step – Δt [s]	1.0x10^{-4}

Table 4. Material properties and time step adopted in the toss rule analysis.

Control mesh (Lxhxz)	Continuity class	Spectral radius - r_∞	Polinomial degrees (p, q, r)
66x3x2	C^1	0,50; 0,95; 0,99;1,00	5, 2, 2
66x3x2	C^2	0,50; 0,95; 0,99;1,00	5, 2, 2
66x3x2	C^3	0,50; 0,95; 0,99;1,00	5, 2, 2
66x3x2	C^4	0,50; 0,95; 0,99;1,00	5, 2, 2

Table 5. Computational parameters employed in the toss rule analysis.

In Fig. 6, the evolution of the different energy variables during the dynamic analysis of the toss rule is presented as function of the spectral radius (r_∞) and continuity class (C^n). The results shown here demonstrate again a sudden interruption of the time integration process when a spectral radius of $r_\infty = 1.00$ is considered (no numerical dissipation), independently of the continuity class utilized. In this sense, the influence of the continuity class on the energy response was not identified. On the other hand, stable solutions can be obtained even with small amounts of numerical dissipation, i.e. $r_\infty = 0.99$, where the total energy is perfectly maintained during the time interval of the numerical analysis. The same behavior was observed for the components of the angular and linear momenta (not presented in this work), which indicates that the formulation proposed in this work presents excellent performance with respect to numerical stability associated with the time integration process. The range of stable spectral radii obtained with the isogeometric model is slightly wider that that presented

by the finite element model proposed by Braun and Awruch (2008). The energy responses obtained here are in agreement with the numerical predictions presented by Kuhl and Ramm (1999).

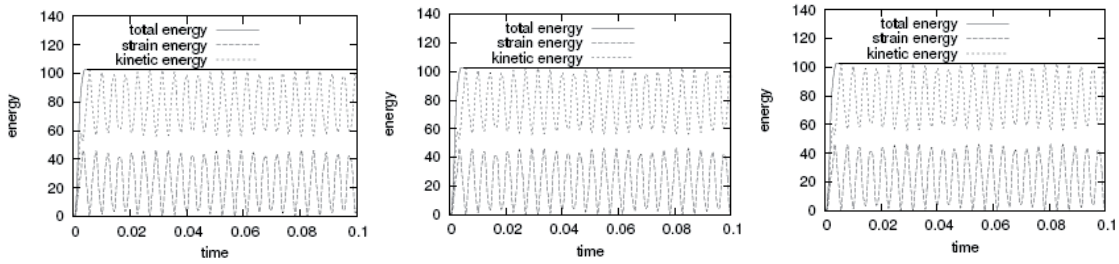

$r_\infty = 0.50$; C^1 $r_\infty = 0.95$; C^1 $r_\infty = 0.99$; C^1

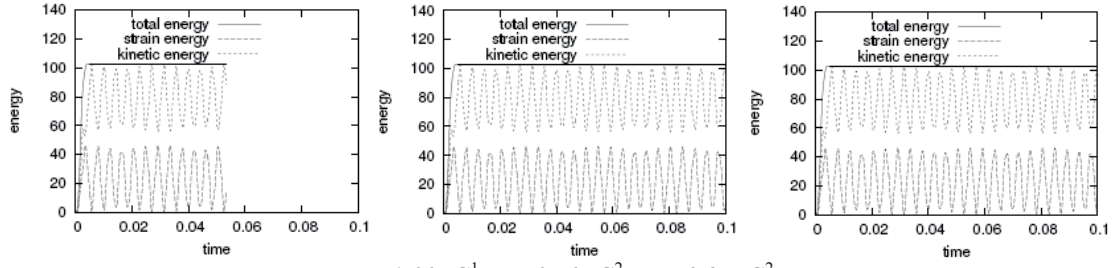

$r_\infty = 1.00$; C^1 $r_\infty = 0.50$; C^2 $r_\infty = 0.95$; C^2

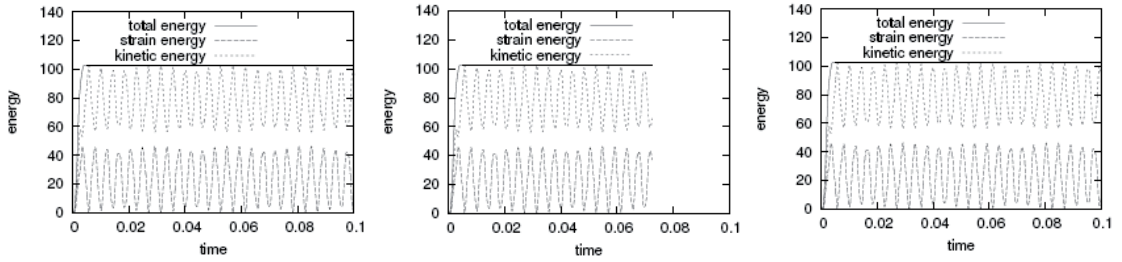

$r_\infty = 0.99$; C^2 $r_\infty = 1.00$; C^2 $r_\infty = 0.50$; C^3

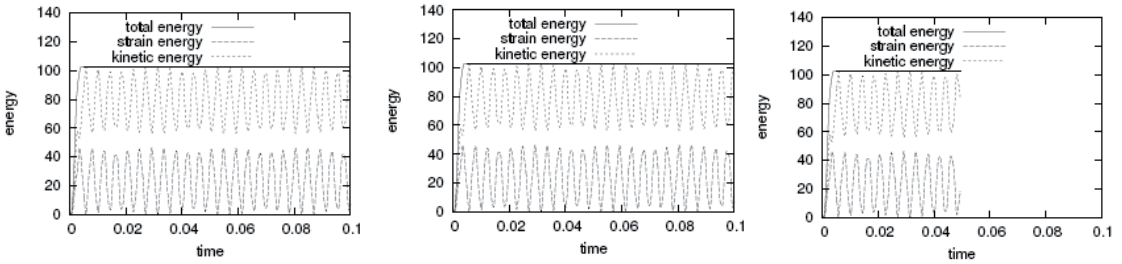

$r_\infty = 0.95$; C^3 $r_\infty = 0.99$; C^3 $r_\infty = 1.00$; C^3

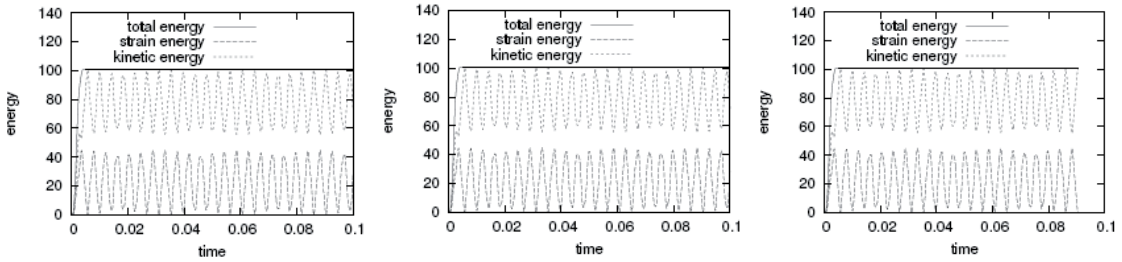

$r_\infty = 0.50$; C^4 $r_\infty = 0.95$; C^4 $r_\infty = 0.99$; C^4

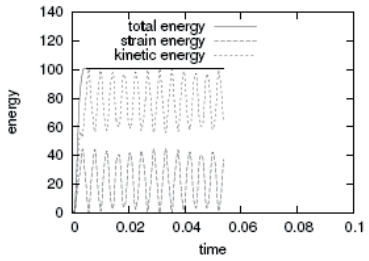

$r_\infty = 1.00$ and C^4

Figure 6. Energy responses for the motion analysis of the toss rule using different combinations of spectral radius (r_∞) and continuity class (C^n).

The motion referring to the toss rule can be visualized in Fig. 7, where a sequence of deformed configurations obtained with the algorithm proposed in this paper is shown. One can observe that the inertial motion is developed after the initial load is removed. Structural displacements take place on the plane *x-z* in accordance with the load configuration prescribed initially.

$r_\infty = 0.95$ and C^4

$r_\infty = 0.95$ and C^1

Figure 7. Deformed configurations of the rule during numerical analysis.

4.3 Cylindrical shell

The snap-through phenomenon occurring in a hinge-supported cylindrical shell subject to a concentrated load is investigated here. Geometrical and load characteristics referring to the present analysis are shown in Fig. 8 and material properties of the structure as well as the time step adopted in the time integration procedure are found in Table 6. Information on computational parameters utilized in the parametric studies carried out here are summarized in Table 7. Number and distribution (LxWxh) of elements over the physical space referring to the cylindrical shell are given as follows: the continuity class C^1 corresponds to the continuity class employed over the shell surface, where the element configuration (8x8) is adopted. The computational mesh related to the continuity class C^4 presents (4x4) elements over the shell surface. Along the shell thickness, two elements of C^0 continuity are used in both meshes, such that the control points associated with the middle surface of the cylindrical shell become interpolatory and the boundary conditions corresponding to hinge supports can be appropriately imposed.

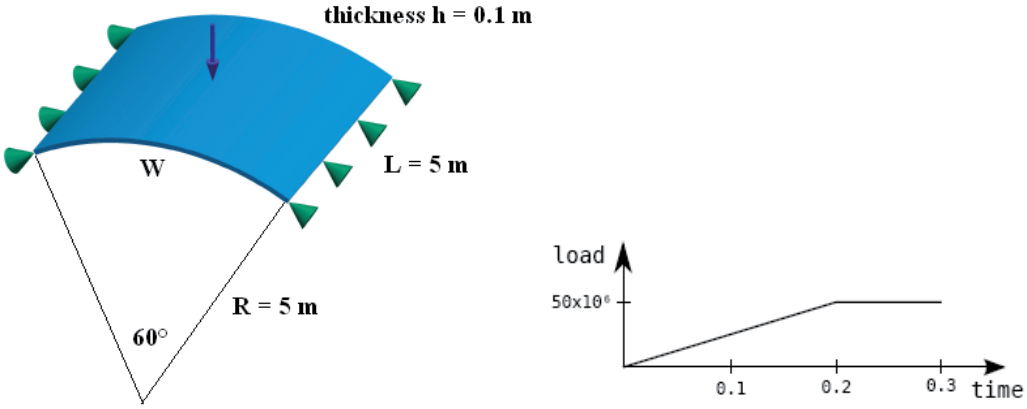

Figure 8. Geometrical and load characteristics for the cylindrical shell analysis.

Young modulus – E [N/m^2]	2x10^{11}
Poisson coefficient – ν	0.25
Specific mass – ρ [Kg/m^3]	1x10^4
Damping coefficient – φ	0.0
Time step – Δt [s]	5.0x10^{-4}

Table 6. Material properties and time step utilized in the cylindrical shell analysis.

Control mesh (LxWxh)	Continuity class	Spectral radius - r_∞	Polinomial degrees (p, q, r)
13x13x5	C^1	0.50; 0.90; 0.95	5, 5, 2
13x13x5	C^4	0.50; 0.90; 0.95	5, 5, 2

Table 7. Computational parameters employed in the cylindrical shell analysis.

Figure 9 presents the dynamic responses obtained in the present analyses with the formulation proposed in this work, which are given in terms of vertical displacements measured at the position where the load is applied. In addition, the displacement response is also evaluated at the middle point on the free edge of the cylindrical shell. One can observe that the continuity class has a minor influence on the dynamic responses obtained here. On the other hand, the effects induced by the spectral radius are clearly noted, since the displacements are continuously increasing for $r_\infty = 0.90$ and $r_\infty = 0.95$. A stable solution is obtained for $r_\infty = 0.50$, although numerical damping can be also observed. It is important to notice that numerical dissipation is identified in this case considering that the amplitude of the displacement response is gradually reduced after the onset of the buckling phenomenon, when a dynamic response with high frequencies is observed. This behavior generally leads to numerical instability if a stabilization strategy with numerical dissipation is not included in the time discretization scheme employed during the time integration. Nevertheless, the amount of numerical damping must be carefully controlled in order to obtain accurate results.

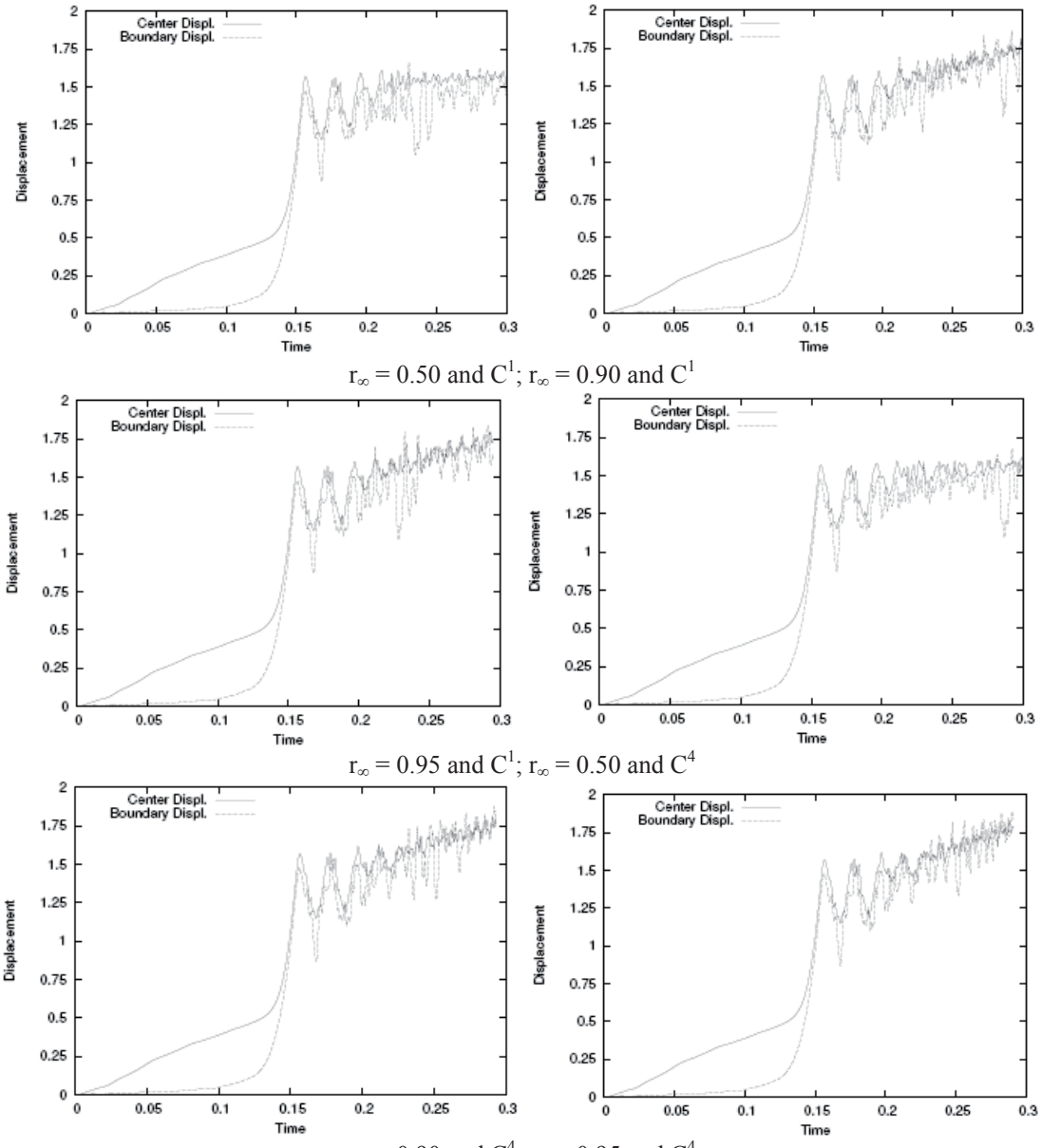

Figure 9. Displacement responses for the cylindrical shell analysis using different combinations of spectral radius (r_∞) and continuity class (C^n).

In Fig. 9, results obtained in this work are compared with numerical predictions obtained by Khul and Ramm (1996, 1999), Balah and Al-Ghamedy (2005) and the commercial package ABAQUS. The present results correspond to the numerical analysis performed considering a spectral radius of $r_\infty = 0.50$ and continuity class C^1. A good agreement can be observed, except for the solution presented by Khul and Ramm (1996), where the higher modes are not present and the energy is concentrated on the lower modes (displacements with larger amplitude).

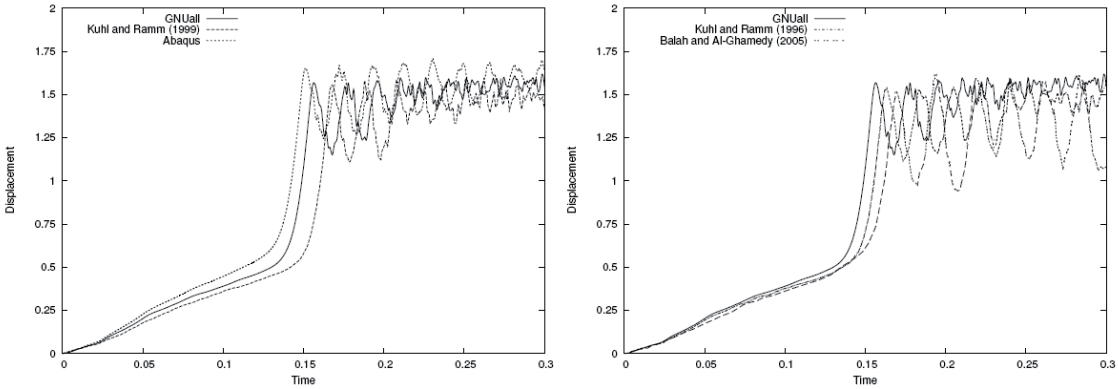

Figure 10. Displacement response of the cylindrical shell obtained from different authors.

Figure 11 shows some configurations assumed by the cylindrical shell during the numerical simulation, where the mesh configuration corresponding to the continuity class C^1 and spectral radius of $r_\infty = 0.50$ were adopted. The buckling phenomenon can be identified and the different stages of deformation are well reproduced, especially for the region near the point where the load is applied.

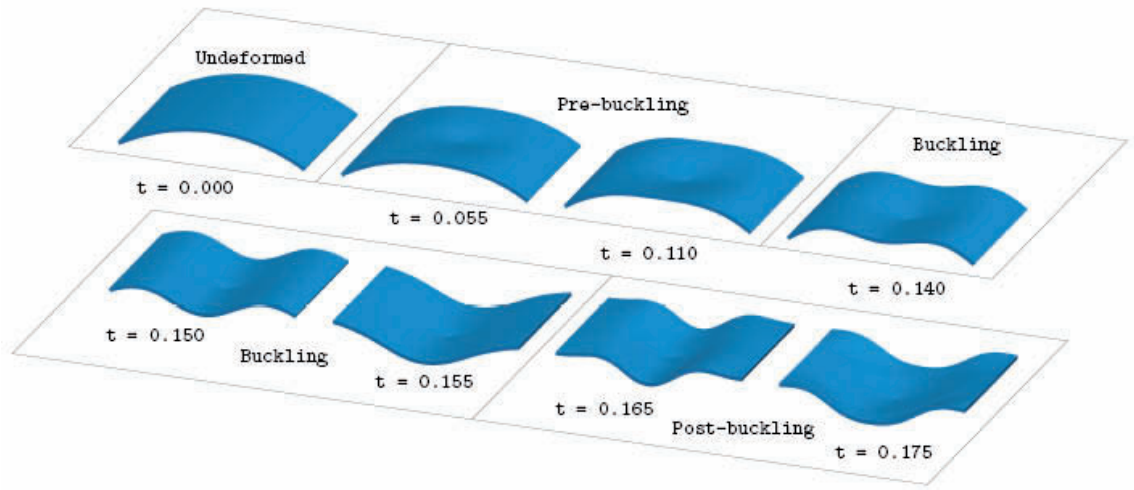

Figure 11. Deformation of the cylindrical shell during dynamic analysis.

5 CONCLUSIONS

A parametric study was performed in this work in order to evaluate the performance of isogeometric analysis for applications on nonlinear elastodynamics. A numerical model for linear and nonlinear dynamic analysis was described considering an isogeometric formulation based on B-splines and NURBS. In order to stabilize the time integration procedure in the nonlinear range, a dissipative energy-momentum conserving method was adopted. The simulations carried out here obtained stable solutions when appropriate numerical dissipation was employed. Conservation of energy and angular as well as linear momentum were shown through the examples. Results demonstrated that isogeometric analysis can provide numerical predictions accurately with much less numerical dissipation than that required by a finite element model previously developed by the present authors with similar characteristics. Moreover, the range of stable spectral radii is wider when isogeometric analysis is utilized. Other important aspect related to isogeometric analysis are the mathematical characteristics of the NURBS basis functions, which leads to better approximations for the modes of vibration

observed in the dynamic analyses. Studies performed with respect to the continuity class of the basis functions indicated that this aspect has a minor influence on the solutions obtained with the present formulation. For future works, the present formulation will be extended in order to deal with applications involving hyperelastic and elastoplastic constitutive models.

REFERENCES

Armero, F., and Petocz, E., Formulation and analysis of conserving algorithms for frictionless dynamic contact-impact problems. *Computer Methods in Applied Mechanics and Engineering*, 158:269-300, 1998.

Armero, F., and Romero, I., On the formulation of high-frequency dissipative time-stepping algorithms for nonlinear dynamics. Part I: low order methods for two model problems and nonlinear elastodynamics. *Computer Methods in Applied Mechanics and Engineering*, 190:2603–2649, 2001a.

Armero, F. and Romero, I., On the formulation of high-frequency dissipative time-stepping algorithms for nonlinear dynamics. Part II: high order methods. *Computer Methods in Applied Mechanics and Engineering*, 190:6783–6824, 2001b.

Balah, M., and Al-Ghamedy, H.N., Energy-momentum conserving algorithm for nonlinear dynamics of laminated shells based on a third-order shear deformation theory. *Journal of Engineering Mechanics ASCE*, 131:12-22, 2005.

Bathe, K.J., *Finite Element Procedures*. Prentice Hall, 1996.

Bathe, K.J., and Baig, M.M.I., On a composite implicit time integration procedure for nonlinear dynamics. *Computers and Structures*, 83:2513-2524, 2005.

Bazilevs, Y., Calo, V.M., Cotrell, J.A., Hughes, T.J.R., Reali, A., and Scovazzi, G., Variational multiscale residual-based turbulence modeling for large eddy simulation of incompressible flows. *Computer Methods in Applied Mechanics and Engineering*, 197:173-201, 2007.

Belytschko, T., and Schoeberle, D.F., On the unconditional stability of an implicit algorithm for nonlinear structural dynamics. *ASME Journal of Applied Mechanics*, 17:865-869, 1975.

Benson, D.J., Bazilevs, Y., Hsu, M.C., and Hughes, T.J.R., Isogeometric shell analysis: The Reissner-Mindlin shell. *Computer Methods in Applied Mechanics and Engineering*, 199, 276-289, 2010.

Braun, A.L., and Awruch, A.M., Geometrically non-linear analysis in elastodynamics using the eight-node finite element with one-point quadrature and the generalized-α method. *Latin American Journal of Solid and Structures*, 5:17-45, 2008.

Chung, J., and Hulbert, G.M., A time integration algorithm for structural dynamics with improved numerical dissipation: the generalized-α method. *Journal of Applied Mechanics, Transactions of the ASME*, 60:371-375, 1993.

Cottrell, J.A., Hughes, T.J.R., and Bazilevs, Y., *Isogeometric Analysis: Towards Integration of CAD and FEA*. Wiley, 2009.

Cox, M.G., The numerical evaluation of B-splines. *Technical report*, National Physics Laboratory, DNAC 4, 1971.

Crisfield, M.A., Galvanetto, U., and Jelenic, G., Dynamics of 3-D co-rotational beams, *Computational Mechanics*, 20:507-519, 1997.

De Boor, C., On calculation with B-splines. *Journal of Approximation Theory*, 6:50–62, 1972.

Duarte Filho, L.A., and Awruch, A.M., Geometrically nonlinear static and dynamic analysis of shells and plates using the eight-node hexahedral element with one-point quadrature. *Finite Elements in Analysis and Design*, 40:1297-1315, 2004.

Erlicher, S., Bonaventura, L., and Bursi, O.S., The analysis of the generalized-α method for

non-linear dynamic problems. *Computational Mechanics*, 28:83–104, 2002.
Espath, L.F.R., Braun, A.L., and Awruch, A.M., An introduction to isogeometric analysis applied to solid mechanics. *In: Proceeding of ENIEF 2011 - XIX Congreso sobre Métodos Numéricos y sus Aplicaciones*, Rosario, Argentina, 2011.
Gonzalez, G., Exact energy and momentum conserving algorithms for general models in nonlinear elasticity. *Computer Methods in Applied Mechanics and Engineering*, 190:1763-1783, 2000.
Goudreau, G.L., and Taylor, R.L., Evaluation of numerical methods in elastodynamics. *Computer Methods in Applied Mechanics and Engineering*, 2:69-97, 1973.
Hilber, H.M., Hughes, T.J.R., and Taylor, R.L., Improved numerical dissipation for the time integration algorithms in structural dynamics. *Earthquake Engineering and Structural Dynamics*, 5:283-292, 1977.
Hughes, T.J.R., Caughey, T.K., and Liu, W.K., Finite element methods for nonlinear elastodynamics which conserve energy. *Journal of Applied Mechanics*, 45:366-370, 1978.
Hughes, T.J.R., Cottrell, J., and Bazilevs, Y., Isogeometric analysis: cad, finite elements, nurbs, exact geometry and mesh refinement. *Computer Methods in Applied Mechanics and Engineering*, 194:4135–4195, 2005.
Hughes, T.J.R., and Winget, J.M., Finite rotations effect in numerical integration of rate constitutive equations arising in large deformation analysis. *International Journal for Numerical Methods in Engineering*, 15:1862-1867, 1980.
Kiendl, J., Bazilevs, Y., Hsu, M.C., Wüchner, R., and Bletzinger, K.U., The bending strip method for isogeometric analysis of Kirchhoff-Love shell structures comprised of multiple patches. *Computer Methods in Applied Mechanics and Engineering*, 199:2403-2416, 2010.
Kuhl, D., and Crisfield, M.A., Energy-conserving and decaying algorithms in non-linear structural dynamics. *International Journal for Numerical Methods in Engineering*, 45:569-599, 1999.
Kuhl, D., and Ramm, E., Constraint energy momentum algorithm and its application to nonlinear dynamics of shells. *Computer Methods in Applied Mechanics and Engineering*, 136:293-315, 1996.
Kuhl, D., and Ramm, E., Generalized energy-momentum method for non-linear adaptive shell dynamics. *Computer Methods in Applied Mechanics and Engineering*, 178:343-366, 1999.
Laursen, T.A., and Meng, X.N., A new solution procedure for application of energy-conserving algorithms to general constitutive models in nonlinear elastodynamics. *Computer Methods in Applied Mechanics and Engineering*, 190:6309-6322, 2001.
Malvern, L.E., *Introduction to the Mechanics of a Continuous Medium*. Prentice Hall, Englewood Cliffs, New Jersey, 1969.
Newmark, N.M., A method of computation for structural dynamics. *Journal of Engineering Mechanics ASCE* 85-EM3:67-94, 1959.
Noels, L., Stainier, L., and Ponthot, J.P., An energy-momentum conserving algorithm for non-linear hypoelatic constitutive models. *International Journal for Numerical Methods in Engineering*, 59:83-114, 2004.
Ortiz, M., A note on energy conservation and stability of nonlinear time-stepping algorithms. *Computer and Structures*, 24:167-168, 1986.
Piegl, L., and Tiller, W., *The NURBS Book (Monographs in Visual Communication)*, Second Edition. Springer-Verlag, New York, 1997.
Romero, I., An analysis of the stress formula for energy-momentum methods in nonlinear elastodynamics. *Computational Mechanics*, available online, 2012.
Simo, J.C., and Tarnow, N., The discrete energy-momentum method. Conserving algorithms

for nonlinear elastodynamics. *Journal of Applied Mathematics and Physics*, 43:757-792, 1992.

Wood, W.D., Bossak, M., and Zienkiewicz, O.C., An alpha modification of Newmark's method. *International Journal for Numerical Methods in Engineering*, 15:1562-1566, 1980.